

## Superaromatic terpyridines based on corannulene responsive to metal ions†

Cite this: *Dalton Trans.*, 2014, **43**, 1753

Difeng Wu, Tao Shao, Jian Men, Xiaochuan Chen and Guowei Gao\*

Received 24th July 2013,  
Accepted 8th October 2013

DOI: 10.1039/c3dt52013g

www.rsc.org/dalton

Two superaromatic terpyridine ligands (**1** and **2**) incorporating a corannulene unit at the 4'-position are reported. The optical and metal sensing properties of both ligands were investigated by the naked eye, and UV-vis and fluorescence spectroscopy in this work. In **1**, the corannulene motif is directly connected to the 4'-phenylterpyridine domain, while in **2**, the corannulene motif and the 4'-phenylterpyridine domain are separated by an acetylene linker. Both **1** and **2** can work as chemosensors for metal ions and display different optical responses to various metal ions. It is shown that both ligands exhibit a colorimetric sensing ability for Fe<sup>2+</sup> through an obvious color change from colorless to magenta, and this color change can be observed easily by the naked eye. The addition of Fe<sup>2+</sup> also leads to significant changes in the absorption spectra of the ligands. A characteristic red shift in the emission spectra is observed in the presence of Zn<sup>2+</sup>, which facilitates the discrimination of Zn<sup>2+</sup> from other metal ions. In addition, density functional theory (DFT) and time-dependent-density functional theory (TD-DFT) calculations were performed and shown to be consistent with the observed experimental results.

## Introduction

In the past decade, the development of chemosensors with high selectivity and sensitivity has been a field of great interest in medical, environmental and biological applications.<sup>1–3</sup> Designing and synthesizing chemosensors that can detect various metal ions has attracted huge attention from chemists.<sup>4,5</sup> Fe<sup>2+</sup> and Zn<sup>2+</sup> play vital roles in many biological processes, such as oxygen transport and metabolism, electron transfer and enzymatic reactions with the mitochondrial respiratory chain. However, disruptions in the normally strict regulation of these ions are responsible for severe systemic disorders, such as anemia, hemochromatosis, Alzheimer's disease and Parkinson's disease.<sup>1,6,7</sup> Thus, the development of an efficient chemosensor for these cations is important for fundamental research and biological applications.

It is well known that terpyridine has a strong and directed metal coordination capacity.<sup>8,9</sup> However, terpyridine itself has not been considered for use as a chemosensor, possibly owing to an expected lack of selectivity (given the diverse range of metal ions it is able to bind) and perhaps also due to its low emission properties.<sup>10,11</sup> Consequently, a number of functionalized terpyridines (especially 4'-substituted terpyridines) have

been designed and synthesized for use as chemosensors.<sup>12–14</sup> Polycyclic aromatic hydrocarbons (PAHs) are ideal candidates to be used as substituents on terpyridine due to their unique electronic and optoelectronic properties. Hexa-*peri*-hexabenzocoronene (HBC), the largest aromatic PAH, was coupled to a terpyridine unit at the 4'-position and the resulting terpyridines displayed intriguing photophysical properties.<sup>15</sup> However, other PAHs have rarely been substituted onto terpyridine until now.

Corannulene is composed of five benzene rings fused to a central five-membered cycle and has a bowl-shaped  $\pi$ -conjugated system, adding one more dimension to the chemistry of the usually planar PAHs.<sup>16,17</sup> Due to their distinct properties, corannulene and its derivatives can be considered as promising building blocks for the construction of functional materials.<sup>18–24</sup> For instance, corannulene derivatives have been shown to emit blue light and are of interest in the fabrication of light emitting diodes.<sup>24</sup> Lithium can be stored/intercalated between corannulenes, yielding a promising anode material for batteries.<sup>21</sup> Liquid crystalline phases that respond to an electric field have also been created using corannulenes.<sup>22</sup> Recently, corannulene connecting to triphenylamine was used as a chemosensor for detecting TNT, which opened up a new area in the applications of corannulene chemistry.<sup>18</sup> However, other corannulene derivatives have rarely been studied as chemosensors, especially for metal ions. Herein, we reported the synthesis and characterization of two superaromatic terpyridine ligands (**1** and **2**) incorporating corannulene units at the

College of Chemistry, Sichuan University, Chengdu, China.

E-mail: gaoguowei@scu.edu.cn; Fax: +86 28 85412095; Tel: +86 28 85412095

†Electronic supplementary information (ESI) available. See DOI: 10.1039/c3dt52013g

4'-position. The photophysical properties of the ligands and their potential applications as chemosensors for metal ions have been investigated.

## Results and discussion

### Synthesis

By far, the most common approach for the construction of 4'-substituted terpyridine is based on the so-called Kröhnke-type condensation reaction.<sup>25,26</sup> In addition, cross-coupling reactions such as the Sonogashira and Suzuki coupling reactions are the most versatile tools for the construction of  $\pi$ -conjugated molecules containing two different units connected *via* acetylene or phenylene linkers.<sup>27,28</sup> Accordingly, the synthesis of the ligands (**1** and **2**) incorporating corannulene units at the 4'-position is illustrated in Scheme 1. 4-Bromobenzaldehyde was employed as the starting material for both ligands. The important precursor bromocorannulene was synthesized *via* bromination of corannulene, which was prepared by the solution phase synthesis.<sup>29,30</sup>

For **1**, in the presence of NaOH and concentrated NH<sub>4</sub>OH, 4-bromobenzaldehyde was reacted with 2-acetylpyridine to afford **3**. In order to generate the acetylene-terminated **4**, **3** was reacted with 2-methyl-3-butyn-2-ol *via* the Sonogashira coupling reaction, followed by a base-promoted deprotection. **4** was isolated in 72% yield following two-step column chromatography. The final transformation also employed Sonogashira coupling between **4** and bromocorannulene in the presence of

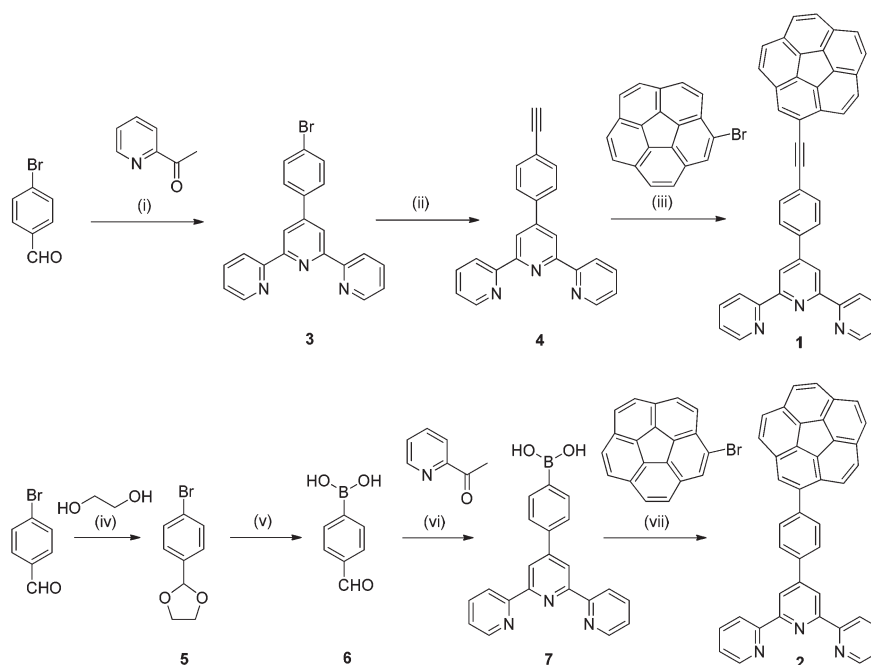
PdCl<sub>2</sub>(PPh<sub>3</sub>)<sub>4</sub> and CuI as catalyst to afford ligand **1** in moderate yield.

In the case of **2**, 4-bromobenzaldehyde was reacted with ethylene glycol employing *p*-toluenesulfonic acid as catalyst to give the ethylene ketal **5**, which was converted into the aryl lithium and then reacted with triisopropyl borate followed by acid hydrolysis to afford **6**. The Kröhnke condensation reaction of **6** with 2-acetylpyridine afforded the important terpyridine precursor **7**, used to generate the target ligand **2** *via* Suzuki coupling with bromocorannulene.

The title compounds were initially characterized on the basis of <sup>1</sup>H, <sup>13</sup>C, elemental and HRMS analysis, which firmly established the structures. The detailed synthetic procedures and spectroscopic data are available in the ESI.†

### UV-vis absorption spectroscopy

The UV-vis absorption studies of **1** and **2** were carried out in a THF-CH<sub>3</sub>CN (*v*:*v* = 1:19) solution at a moderate concentration (1.0 × 10<sup>-5</sup> mol L<sup>-1</sup>). As shown in Fig. 1 and Table 1, compound **2** exhibited a strong absorption band at 282 nm ( $\epsilon = 3.74 \times 10^4$  L mol<sup>-1</sup> cm<sup>-1</sup>) and a shoulder band at 295 nm ( $\epsilon = 3.23 \times 10^4$  L mol<sup>-1</sup> cm<sup>-1</sup>), which are assigned to the  $\pi$ - $\pi^*$  transition within the compound. For compound **1**,  $\pi$ - $\pi^*$  bands at 284 nm ( $\epsilon = 4.23 \times 10^4$  L mol<sup>-1</sup> cm<sup>-1</sup>) were also observed, but the corresponding shoulder band increased and was red-shifted to 303 nm ( $\epsilon = 4.53 \times 10^4$  L mol<sup>-1</sup> cm<sup>-1</sup>). This could be attributed to the fact that the introduction of acetylene linkage extended the molecular conjugation and reduced the flexibility of the single bond connection, resulting in a more delocalized



**Scheme 1** Synthetic route to **1** and **2**. Reagents and conditions: (i) NaOH, NH<sub>4</sub>OH, EtOH, reflux, 4 h, 60%; (ii) (a) 2-methyl-3-butyn-2-ol, PdCl<sub>2</sub>(PPh<sub>3</sub>)<sub>2</sub>, PPh<sub>3</sub>, CuI, Et<sub>3</sub>N, THF, reflux, 12 h, (b) KOH, toluene, reflux, 1 h, 72% overall; (iii) PdCl<sub>2</sub>(PPh<sub>3</sub>)<sub>2</sub>, PPh<sub>3</sub>, CuI, Et<sub>3</sub>N, reflux, 24 h, 55%; (iv) TsOH, toluene, reflux, 24 h, 86%; (v) (a) *n*-BuLi, B(OiPr)<sub>3</sub>, THF, -78 °C to r.t. overnight, (b) 3 N HCl, THF, r.t., 2 h, 71% overall; (vi) (a) NaOH, EtOH, 25 °C, 7 h, (b) NH<sub>4</sub>OH, 65 °C, 12 h, 72% overall; (vii) Pd(PPh<sub>3</sub>)<sub>4</sub>, Na<sub>2</sub>CO<sub>3</sub>, toluene, CH<sub>3</sub>OH, reflux, 24 h, 64%.

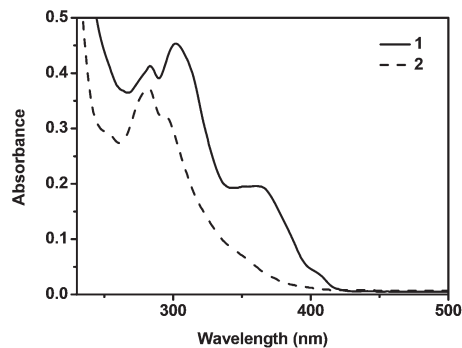


Fig. 1 UV-vis absorption spectroscopy of **1** and **2** (10  $\mu\text{M}$ ) in THF- $\text{CH}_3\text{CN}$  ( $v:v = 1:19$ ) solution.

Table 1 UV-vis absorption, emission and quantum yields for **1** and **2**<sup>a</sup>

Entry	Absorption $\lambda_{\text{max}}/\text{nm}$ ( $\log \epsilon$ )	Emission $I_{\text{max}}^b/\text{nm}$	$\Phi^c$
1	284 (4.63), 303 (4.66), 364 (4.29)	416, 437	0.19
2	282 (4.57), 295 (4.51)	437	0.16

<sup>a</sup> Measurements recorded in THF- $\text{CH}_3\text{CN}$  ( $v:v = 1:19$ ) solution.

<sup>b</sup> Excitation wavelengths were fixed at 300 nm for **1** and 295 nm for **2**.

<sup>c</sup> Fluorescence quantum yields were measured relative to corannulene,  $\Phi = 0.07$ .

$\pi$  system. In addition, there is a new shoulder band at 364 nm ( $\epsilon = 1.97 \times 10^4 \text{ L mol}^{-1} \text{ cm}^{-1}$ ), which is not observed in the spectrum of **2**.

### Emission spectroscopy

Luminescence spectra were recorded for **1** and **2** in a THF- $\text{CH}_3\text{CN}$  ( $v:v = 1:19$ ) solution at a concentration of  $1.0 \times 10^{-5} \text{ mol L}^{-1}$ . For both compounds, their spectrum consists of a characteristic broad band at  $\sim 400\text{--}600 \text{ nm}$  (shown in Fig. 2 and Table 1).

For **1**, the most intense peak within this band occurs at 437 nm, but another peak at 416 nm also dominates the spectrum. In the case of **2**, the most intense peak within the emission band is only observed at 437 nm, which is relatively less intense as compared to the corresponding peaks in **1**. The fluorescence quantum yields of **1** and **2** were measured in

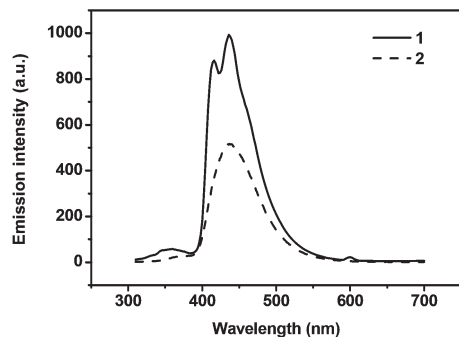


Fig. 2 Emission spectroscopy of **1** and **2** (10  $\mu\text{M}$ ) in a THF- $\text{CH}_3\text{CN}$  ( $v:v = 1:19$ ) solution ( $\lambda_{\text{ex}} = 300 \text{ nm}$  for **1** and 295 nm for **2**).

THF- $\text{CH}_3\text{CN}$  ( $v:v = 1:19$ ) by comparison with a solution of corannulene ( $\Phi = 0.07$ ).<sup>31</sup> As shown in Table 1, the quantum yield of **1** was found to be approximately 0.19, which is higher than that of **2** (*ca.* 0.16). This can be attributed to the presence of the acetylene bridge which facilitates electron and energy transfer, resulting in a more efficient internal conversion process in **1**.<sup>15</sup>

### Cation-sensing studies

As terpyridine is a well-known metal chelating unit, we wondered if **1** and **2** could be used as a chemosensor for metal ions. The chemosensor behavior of **1** and **2** with a variety of metal cations ( $\text{Na}^+$ ,  $\text{K}^+$ ,  $\text{Mg}^{2+}$ ,  $\text{Ba}^{2+}$ ,  $\text{Al}^{3+}$ ,  $\text{Mn}^{2+}$ ,  $\text{Fe}^{2+}$ ,  $\text{Fe}^{3+}$ ,  $\text{Co}^{2+}$ ,  $\text{Ni}^{2+}$ ,  $\text{Zn}^{2+}$  and  $\text{Cd}^{2+}$ ) were investigated by visual examination, UV-vis and fluorescence measurements.

**Colorimetric signaling.** The sensing ability of the metallo-receptors towards various cations was studied qualitatively by visual examination of the cation-induced color and the fluorescence changes of the receptors in THF solution. As exemplified in Fig. 3, upon the addition of one equivalent of  $\text{Fe}^{2+}$  ions to the solution of **1**, the color in daylight (Fig. 3a) of the solutions changes drastically from colorless to purple. In contrast, the addition of other metal cations has little effect on the color of the solution of **1**. A similar phenomenon is also observed for **2** (Fig. 3c). It is important to note that color change is one of the most convenient visual detection methods used in classical chemical analysis, as well as being straight-forward and inexpensive. The results indicate that both **1** and **2** can serve as sensitive “naked-eye” indicators for  $\text{Fe}^{2+}$  ions.

In addition, chelation experiments showed that the response is irreversible. The addition of the well-known cation chelator, ethylenediamine tetraacetic acid (EDTA), did not recover a colorless solution of the ligands, indicating the strong coordination ability of these ligands to  $\text{Fe}^{2+}$ .

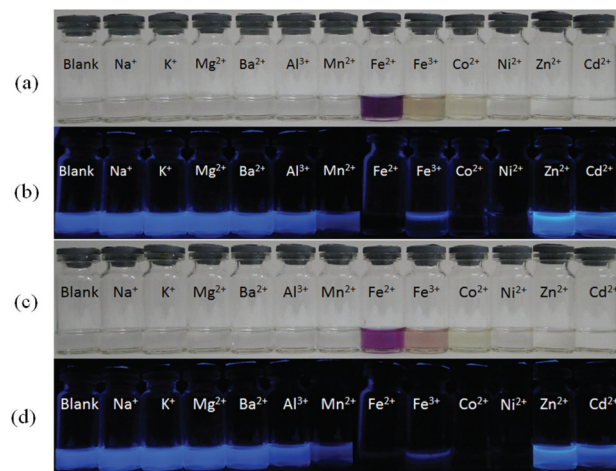


Fig. 3 Photographs of **1** and **2** in THF solution (200  $\mu\text{M}$ ) in the presence of different metal cations (1.0 eq.): (a) daylight for **1**; (b) UV light for **1**; (c) daylight for **2**; (d) UV light for **2**.

Under UV illumination (Fig. 3b and 3d), both **1** and **2** exhibit cyan fluorescence in THF solution. The presence of  $\text{Zn}^{2+}$  slightly enhances the fluorescence of the solution. However, the group VIIIIB metal ions ( $\text{Fe}^{2+}$ ,  $\text{Fe}^{3+}$ ,  $\text{Co}^{2+}$  and  $\text{Ni}^{2+}$ ) and  $\text{Mn}^{2+}$  ions are found to efficiently quench the emission. The dramatic cation-specific response makes the receptors especially effective colorimetric cation sensors.

**Absorption signaling.** The sensing of the receptors towards various cations in THF- $\text{CH}_3\text{CN}$  ( $v:v = 1:19$ ) was studied through UV-vis spectroscopy. As shown in Fig. 4, the addition of one equivalent of  $\text{Na}^+$ ,  $\text{K}^+$ ,  $\text{Mg}^{2+}$ ,  $\text{Ba}^{2+}$  and  $\text{Al}^{3+}$  ions to the solution of **1** induced little change in the absorption spectra of **1** and **2**. In contrast, when exposed to  $\text{Mn}^{2+}$ ,  $\text{Co}^{2+}$ ,  $\text{Ni}^{2+}$ ,  $\text{Zn}^{2+}$  and  $\text{Cd}^{2+}$  ions, the absorbance intensity at 303 nm decreased and simultaneously, the absorption shoulder bands around 373 nm increased. Interestingly, the addition of  $\text{Fe}^{2+}$  induced the appearance of a metal-to-ligand charge transfer (MLCT) band centered at 574 nm due to the  $\text{Fe}^{2+}$  ion coordination to **1**.<sup>32</sup> In the case of **2**, the addition of  $\text{Na}^+$ ,  $\text{K}^+$ ,  $\text{Mg}^{2+}$ ,  $\text{Ba}^{2+}$  and  $\text{Al}^{3+}$  ions induced the increase or decrease of the absorbance at 295 nm with no appearance of any additional bands. Other metal ions apart from  $\text{Fe}^{2+}$  not only decreased the absorbance intensity at 295 nm, but also exhibited absorption shoulder bands around 326 nm. In contrast, the addition of  $\text{Fe}^{2+}$  led to significant changes in the absorption spectra. An absorption peak at 571 nm appeared upon the addition of  $\text{Fe}^{2+}$ . The above results reveal the unique absorbance featured by both ligands which is induced by coordination with  $\text{Fe}^{2+}$ , giving rise to the solution color change from colorless to purple. Moreover, the

addition of other metal ions such as  $\text{Na}^+$ ,  $\text{K}^+$ ,  $\text{Mg}^{2+}$ ,  $\text{Ba}^{2+}$ ,  $\text{Al}^{3+}$ ,  $\text{Mn}^{2+}$ ,  $\text{Fe}^{3+}$ ,  $\text{Co}^{2+}$ ,  $\text{Ni}^{2+}$ ,  $\text{Zn}^{2+}$  and  $\text{Cd}^{2+}$  cannot produce the significant changes in the UV-vis spectra observed for the solution of  $\text{Fe}^{2+}$  ions and the ligands. This indicates that both terpyridine ligands have high selectivity for  $\text{Fe}^{2+}$  over other metal ions. Therefore, they both have potential as  $\text{Fe}^{2+}$  chemosensors through UV-vis spectrometry.

To further determine the stoichiometry and binding ability of our chemosensors toward  $\text{Fe}^{2+}$ , titration experiments were performed as shown in Fig. 5. Upon the addition of 0–1.5 eq. of  $\text{Fe}^{2+}$  cations to **1**, the absorption intensity of the  $\pi$ - $\pi^*$  bands at 303 nm gradually weakened while simultaneously, the absorption shoulder bands around 373 nm and the MLCT band at 574 nm increased progressively, resulting in an isosbestic point at 322 nm. The variation of  $A_{574 \text{ nm}}/A_{303 \text{ nm}}$  with the molar fraction of  $\text{Fe}^{2+}$  (Fig. 5, top, inset) indicated that the binding of **1** with  $\text{Fe}^{2+}$  showed a 1 : 1 stoichiometry. In the case of **2**, upon the addition of  $\text{Fe}^{2+}$ , two new bands centered at 571 nm and 322 nm appeared while the band at 295 nm disappeared gradually. The ratio of  $A_{571 \text{ nm}}/A_{303 \text{ nm}}$  against the molar fraction of  $\text{Fe}^{2+}$  (Fig. 5, bottom, inset) also indicated that the binding of **2** with  $\text{Fe}^{2+}$  showed a 1 : 1 stoichiometry.

The binding stoichiometry of **1** and **2** with  $\text{Fe}^{2+}$  ions was further estimated using the Benesi-Hildebrand equation,<sup>33</sup>

$$1/(A - A_0) = 1/(A - A_\infty) \times [1/K[\text{Fe}^{2+}]^n + 1] \quad (1)$$

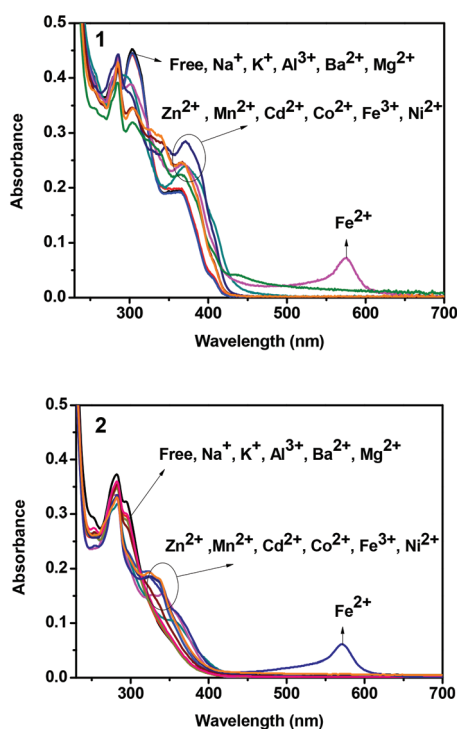


Fig. 4 Absorption spectra of **1** and **2** (10  $\mu\text{M}$ ) in THF- $\text{CH}_3\text{CN}$  ( $v:v = 1:19$ ) induced by various metal cations (1.0 eq.).

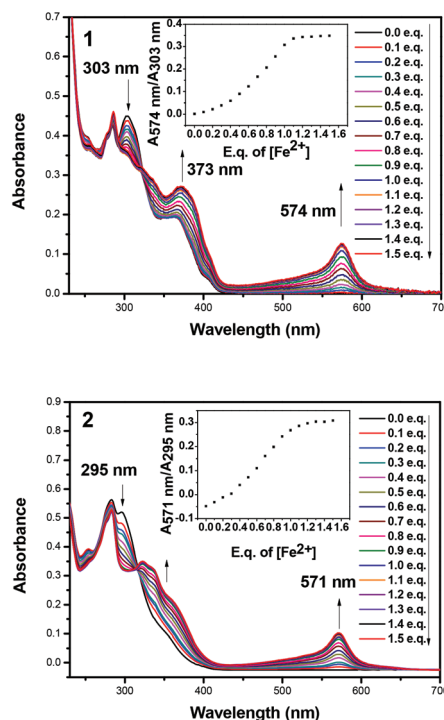


Fig. 5 Changes in the UV-vis absorption spectra of **1** and **2** in a THF-acetonitrile ( $v:v = 1:19$ ) solution (10  $\mu\text{M}$ ) upon titration (0–15  $\mu\text{M}$ ) of  $\text{Fe}^{2+}$ . Inset: titration curve of **1** and **2** with  $\text{Fe}^{2+}$  (the absorbance ratio at 574 nm and 303 nm for **1** and at 571 nm and 295 nm for **2**).

**Table 2** The association constants of  $\text{Fe}^{2+}$ ,  $\text{Zn}^{2+}$  and  $\text{Cd}^{2+}$  to **1** and **2**, calculated using the Benesi–Hildebrand equation

Entry	<b>1</b>		<b>2</b>	
	$\lambda^a$ (nm)	$K$ ( $\text{M}^{-1}$ )	$\lambda^a$ (nm)	$K$ ( $\text{M}^{-1}$ )
$\text{Fe}^{2+}$	303	$4.73 \times 10^4$	295	$1.42 \times 10^5$
$\text{Zn}^{2+}$		$8.92 \times 10^3$		$1.50 \times 10^4$
$\text{Cd}^{2+}$		$3.89 \times 10^3$		$5.16 \times 10^3$

<sup>a</sup>The most changed wavelength selected for the Benesi–Hildebrand plot.

where  $A_0$  is the absorbance of free **1** or **2**,  $A_\infty$  is the absorbance measured with excess amounts of  $\text{Fe}^{2+}$ ,  $A$  is the absorbance measured with  $\text{Fe}^{2+}$ ,  $n$  represents the binding stoichiometry of  $\text{Fe}^{2+}$  to **1** or **2**,  $K$  is the association constant and  $[\text{Fe}^{2+}]$  is the concentration of  $\text{Fe}^{2+}$ .

As shown in Fig. S4.1,† the plot of  $1/(A - A_0)$  against  $1/[\text{Fe}^{2+}]$  shows a linear relationship ( $R = 0.9959$ ), indicating that **1** associates with  $\text{Fe}^{2+}$  in a 1:1 stoichiometry. The association constant,  $K$ , between **1** and  $\text{Fe}^{2+}$ , was determined from the ratio of the intercept to the slope to be  $4.73 \times 10^4 \text{ M}^{-1}$ . Similar phenomena were observed in the association of **2** with  $\text{Fe}^{2+}$ . The binding constant was estimated as  $1.42 \times 10^5 \text{ M}^{-1}$ , which was larger than the value for **1**. This can be attributed to the fact that the introduction of acetylene linkage enhances the conjugation of the molecule and thus reduces the coordination ability of the N atom of terpyridine in **1**.<sup>15,34</sup>

These observations were reinforced by the results of the addition of  $\text{Zn}^{2+}$  or  $\text{Cd}^{2+}$  to the solution of our ligands (Fig. S4.2, S4.3† and Table 2). The association constants of  $\text{Zn}^{2+}$  and  $\text{Cd}^{2+}$  to **1** were calculated as  $8.92 \times 10^3 \text{ M}^{-1}$  and  $3.89 \times 10^3 \text{ M}^{-1}$ , which are smaller than the values of  $\text{Zn}^{2+}$  ( $1.50 \times 10^4 \text{ M}^{-1}$ ) and  $\text{Cd}^{2+}$  ( $5.16 \times 10^3 \text{ M}^{-1}$ ) to **2**. The results indicate that the coordination ability of terpyridine in **2** is stronger than that in **1**. It is worthy of note that the conjugated size of the substituent group at the 4'-position of terpyridine plays a vital role in the coordination ability of the ligands. Therefore, the introduction of various PAHs with different conjugated sizes could be used for regulating the binding ability of terpyridine, which achieves the aim of enhancing the selectivity and sensitivity of terpyridine sensors for specific metal ions.

The detection limit is one of the most important parameters in cation sensing for practical purposes. Therefore, the limitations of detection (LOD) of our ligands for  $\text{Fe}^{2+}$  were obtained according to the equation: detection limit =  $3\sigma/\text{slope}$ , where  $\sigma$  is the standard deviation of blank measurements, slope is the slope between intensity versus sample concentration.<sup>35</sup> The LOD for  $\text{Fe}^{2+}$  were measured as  $1.1 \times 10^{-7} \text{ M}$  and  $8.9 \times 10^{-8} \text{ M}$  for **1** and **2**, respectively (Fig. S5.1 and S5.2†). These data indicate that our ligands show high sensitivity toward  $\text{Fe}^{2+}$ .

Response time is also an important practical parameter for chemosensors. After the addition of 1.0 equiv. of  $\text{Fe}^{2+}$  to the solutions of the ligands, absorption changes were tracked as a

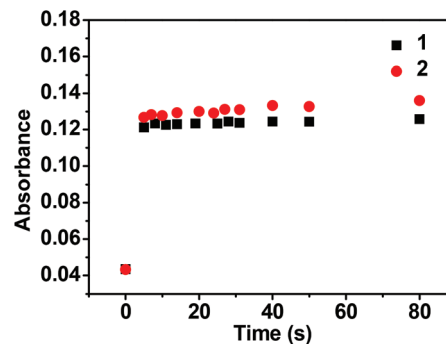


**Fig. 6** Time course of the absorption response of **1** and **2** ( $10 \mu\text{M}$ ) upon the addition of 1.0 equiv. of  $\text{Fe}^{2+}$  in a THF–acetonitrile ( $v:v = 1:19$ ) solution.

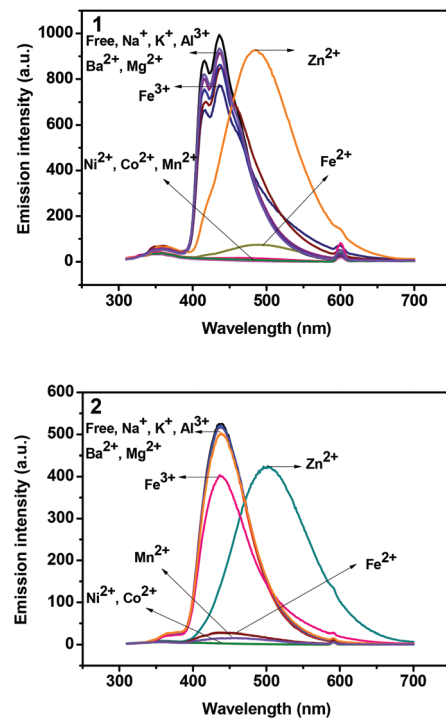


**Fig. 7** Fluorescence emission spectra of **1** and **2** ( $10 \mu\text{M}$ ) upon the addition of various metal ions (1.0 equiv.) in THF–acetonitrile ( $v:v = 1:19$ ) solution ( $\lambda_{\text{ex}} = 300 \text{ nm}$  for **1** and  $295 \text{ nm}$  for **2**).

function of time (Fig. 6), which indicate that rapid response within a few seconds was observed for **1** and **2**.

**Fluorescence signalling.** The fluorescence properties of **1** and **2** upon the addition of several metal ions were also investigated by fluorescence spectroscopic measurements and titration studies. Fig. 7 shows the fluorescence response of **1** and **2** towards various metal ions in THF–acetonitrile ( $v:v = 1:19$ ) solution at  $\lambda_{\text{ex}} = 300 \text{ nm}$  for **1** and  $\lambda_{\text{ex}} = 295 \text{ nm}$  for **2**. In the case of **1**, the addition of  $\text{Na}^+$ ,  $\text{K}^+$ ,  $\text{Mg}^{2+}$ ,  $\text{Ba}^{2+}$ ,  $\text{Al}^{3+}$  and  $\text{Fe}^{3+}$  induced a very minor decrease in the emission band. In the presence of  $\text{Fe}^{2+}$ , the fluorescence decreased obviously, accompanied by the emission band red-shifting to  $488 \text{ nm}$ . Additionally, the presence of  $\text{Ni}^{2+}$ ,  $\text{Co}^{2+}$  and  $\text{Mn}^{2+}$  quenched

the fluorescence almost completely. Interestingly, when  $\text{Zn}^{2+}$  ions were added to the solution of **1**, the fluorescence spectrum of the complex showed a significant bathochromic shift. In the case of **2**,  $\text{Na}^+$ ,  $\text{K}^+$ ,  $\text{Mg}^{2+}$ ,  $\text{Ba}^{2+}$  and  $\text{Al}^{3+}$  could not induce any changes in the emission bands, while the fluorescence was quenched to some extent in the presence of  $\text{Fe}^{3+}$  ions.  $\text{Fe}^{2+}$ ,  $\text{Ni}^{2+}$ ,  $\text{Co}^{2+}$  and  $\text{Mn}^{2+}$  were found to efficiently quench the emission of **2**. When exposed to  $\text{Zn}^{2+}$ , ligand **2** also showed a significant bathochromic emission shift.

The above results reveal the unique fluorescence features of both ligands induced by the coordination with  $\text{Zn}^{2+}$ , implying that our ligands could be used as fluorescence sensors for  $\text{Zn}^{2+}$ . However, one of the most important aspects that should be explored for a sensor is its ability to detect a specific cation in the presence of competing ions. In this case, the selectivity of both ligands for  $\text{Zn}^{2+}$  over other metal ions was revealed by measuring the fluorescence spectra of both ligands with  $\text{Zn}^{2+}$  in the presence of other competitive cations. As shown in Fig. S6,† 2.0 equiv. of competitive cations were added to the complex of **1** or **2** with  $\text{Zn}^{2+}$  and the fluorescence response was detected. All the cations except  $\text{Co}^{2+}$  exhibit only small or no interference with the affinity of our ligands with  $\text{Zn}^{2+}$ . In contrast,  $\text{Co}^{2+}$  ions can almost completely quench fluorescence emission due to the strong affinity of our ligands and  $\text{Co}^{2+}$ . These results confirm that our ligands show a good specificity toward  $\text{Zn}^{2+}$  and hence could be used to detect  $\text{Zn}^{2+}$  ion in a complicated matrix.

To further determine the stoichiometry and detectability of our chemosensors toward  $\text{Zn}^{2+}$ , detailed investigations were carried out and the results are displayed in Fig. 8. With the addition of  $\text{Zn}^{2+}$  to **1** (Fig. 8, top), the intensity of the emission band peaks at 416 nm and 437 nm decreases gradually, while a new emission band emerges with a  $\lambda_{\text{max}}$  located at 495 nm. As a result, an isoemissive point at 459 nm can be found. The intensity ratio at 495 nm and 437 nm increases with the incremental addition of  $\text{Zn}^{2+}$  until  $[\text{Zn}^{2+}]/[\mathbf{1}]$  reaches 1.0. Even higher concentrations of  $\text{Zn}^{2+}$  do not lead to any further change. This indicates that the **1**- $\text{Zn}^{2+}$  complex is formed in approximately 1:1 stoichiometry. The fluorimetric limitation of detection (LOD) for **1** with  $\text{Zn}^{2+}$  is determined to be  $\sim 1.6 \times 10^{-8}$  M (Fig. S5.3†).<sup>35</sup> A similar situation is found in the addition of  $\text{Zn}^{2+}$  to **2** (Fig. 8, bottom). The fluorimetric LOD for **2** with  $\text{Zn}^{2+}$  is determined to be  $\sim 2.0 \times 10^{-8}$  M (Fig. S5.4†). The addition of increasing amounts of  $\text{Zn}^{2+}$  to **2** induces a red-shift of 63 nm in the emission peak from 437 to 500 nm. The intensity ratio at 500 and 437 nm ( $I_{500 \text{ nm}}/I_{437 \text{ nm}}$ ) increases from 0.27 to 3.09 and the stoichiometry of the coordinating species is also found to be 1:1 according to the variation of  $I_{500 \text{ nm}}/I_{437 \text{ nm}}$  with the molar fraction of  $\text{Zn}^{2+}$ . In addition, Job's plot analysis also demonstrates a 1:1 binding stoichiometry between our ligands and  $\text{Zn}^{2+}$  (Fig. S7†). That the binding of  $\text{Zn}^{2+}$  to ligands leads to red-shifts is not surprising, since the positive charge on the metal ion will promote the intramolecular charge transfer (ICT) process from pendant corannulene to terpyridine.<sup>10,11</sup> It is worth noting that such ratiometric fluorimetry, where the ratio of signals at two emission wavelengths

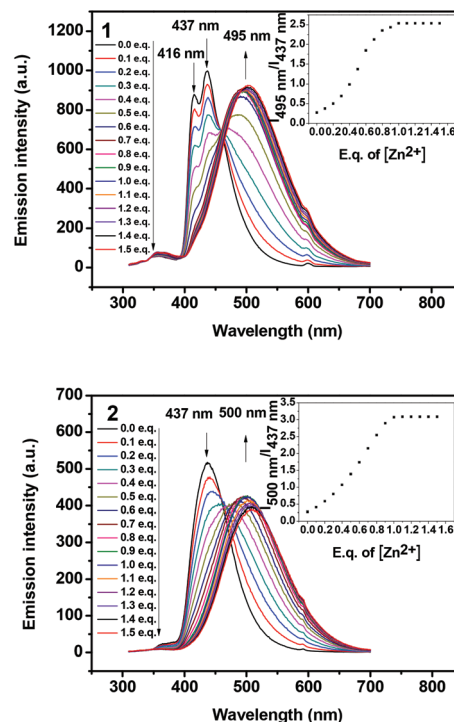


Fig. 8 Fluorescence emission spectra of **1** and **2** (10  $\mu\text{M}$ ) in THF-acetonitrile ( $v:v = 1:19$ ) solution upon titration of  $\text{Zn}^{2+}$  (0–15  $\mu\text{M}$ ). Inset: titration curve of **1** and **2** with  $\text{Zn}^{2+}$  (intensity ratio at 495 nm and 437 nm for **1**; ratio at 500 nm and 437 nm for **2**).

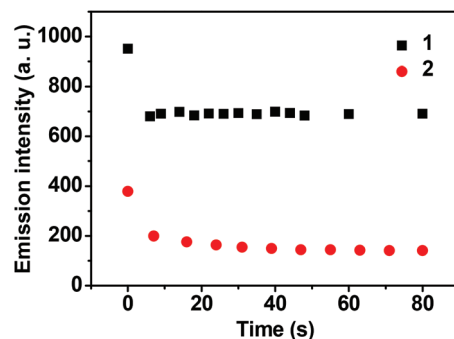


Fig. 9 Time course of the fluorescence response of **1** and **2** (10  $\mu\text{M}$ ) upon the addition of 1 equiv. of  $\text{Zn}^{2+}$  in THF-acetonitrile ( $v:v = 1:19$ ) solution.

is monitored, is highly desirable in practical sensors, in order to cancel out variations in intensity arising from background changes in the analytical environment. In addition, the response time of our ligands for  $\text{Zn}^{2+}$  was also studied. As shown in Fig. 9, only 5 s was required for **1** to reach 90% of the saturation fluorescence, and for **2**, the fluorescence intensity reached 90% of the saturation value within 20 s.

**Cation sensing in aqueous  $\text{CH}_3\text{CN}$ -THF solution.** The sensing of cations in aqueous media or water-organic mixed solvents is important for practical applications.<sup>36,37</sup> Therefore, we studied the effect of the content of the aqueous 4-(2-hydroxyethyl)-1-piperazineethanesulfonic acid (HEPES) buffer

(30 mM, pH = 7.4) in CH<sub>3</sub>CN–THF solution on the colorimetric response of our ligands toward ferrous ion. As shown in Fig. S8.1,† when the water content was increased up to a 20–30% volume ratio, the purple color of the solution was still clearly visible, indicating that our ligands acted as effective chemosensors toward the detection of Fe<sup>2+</sup> in the aqueous CH<sub>3</sub>CN–THF solution. Therefore, HEPES buffer–CH<sub>3</sub>CN–THF (4:15:1, v:v:v, pH 7.4) was selected as the water–organic mixed solvent to study the chemosensor behavior of our ligands. In the case of **1**, when 1.0 equiv. of various cations was added, only Fe<sup>2+</sup> triggered a new peak at 574 nm in the absorption spectra while the other cations induced no changes at this wavelength, indicating that ligand **1** can be established as a highly sensitive colorimetric sensor for Fe<sup>2+</sup> in water–organic mixed solvents (Fig. S8.2†). Changes in the luminescence spectrum ( $\lambda_{\text{ex}} = 300$  nm) of **1** (10  $\mu\text{M}$ ) in a HEPES buffer–CH<sub>3</sub>CN–THF (4:15:1, v:v:v, pH 7.4) solution upon the addition of different cations showed that only Zn<sup>2+</sup> could induce a significant bathochromic shift of about 60 nm, implying that ligand **1** can act as a highly sensitive fluorescent Zn<sup>2+</sup> probe in aqueous CH<sub>3</sub>CN–THF solution (Fig. S8.3†). However, competition experiments showed that the sensing properties of **1** for Fe<sup>2+</sup> and Zn<sup>2+</sup> encountered interference by Co<sup>2+</sup>, which was in line with the results observed in organic solvents. Similar measurements for **2** also showed that ligand **2** has a good selectivity toward Fe<sup>2+</sup> and Zn<sup>2+</sup> in aqueous CH<sub>3</sub>CN–THF solution (Fig. S8.2 and S8.3†). Accordingly, our ligands can be used as multichannel sensors for multiple target cations in both organic solvents and water–organic mixed solvents.

### DFT studies

To gain insight into the geometry and optical properties of ligands **1** and **2** we performed density functional theory (DFT) and time-dependent-density functional theory (TD-DFT) calculations on the geometrical configuration and absorption spectrum of **1** and **2**. We employed the B3LYP exchange–correlation functional with a 6-31G\* basis set, as implemented in the Gaussian 09 suite of programs.<sup>38</sup> The B3LYP/6-31G\* geometry optimized structures for **1** and **2** are presented in Fig. 10. In both structures, the connecting phenyl ring (ring 2) and the

central pyridine ring (ring 3) are twisted about 30°, which can be ascribed to the unfavourable interaction between the adjacent protons. Due to the introduction of acetylene linkage in **1**, the phenyl ring in corannulene (ring 1) is calculated to be coplanar with the connecting phenyl ring (ring 2). In contrast, ring 1 in **2** is twisted about 40° with respect to ring 2. This indicates that the introduction of acetylene linkage has led to improvement in the planarity of the ligands.

A schematic representation of the molecular orbitals for **1** and **2** is reported in Fig. 10. In the case of **2**, the electron clouds in the terpyridine unit are mainly concentrated on the central pyridine ring and partly localized on the side pyridine rings. However, in **1**, the electron clouds are only localized on the central pyridine ring. In other words, the electron clouds of the terpyridine unit in **1** are found to be smaller and more shifted towards the corannulene domain in comparison with that of ligand **2**. Therefore, the coordination ability of terpyridine in **2** is stronger than that in **1**, which is in line with the optical titration results. As shown in Fig. 11, the energy gap ( $\Delta E$ ) between the highest occupied molecular orbital (HOMO) and the lowest unoccupied molecular orbital (LUMO) for both ligands was also obtained *via* chemical calculations. The  $\Delta E$  value of **1** is 0.43 eV lower than that of **2**, which can be explained in that the maximum absorption wavelength of ligand **1** is found to be bathochromic with respect to ligand **2**.

TD-DFT calculations were also carried out at the B3LYP level of theory with a 6-31G\* basis set. Calculated wavelengths and oscillator frequencies ( $f$ ) are listed in Table 3. According to TD-DFT calculations for **1**, three significant transitions are predicted to be observed at 403.74 nm ( $f = 1.0101$ ), 383.81 nm ( $f = 0.0022$ ) and 366.46 nm ( $f = 0.2513$ ). In contrast, only two significant transitions for **2** are obtained at 361.95 nm ( $f = 0.0366$ ) and 351.43 nm ( $f = 0.0083$ ). This is in line with the absorption results that there is one more shoulder band in the spectrum of ligand **1** than that of ligand **2**. The calculated wavelengths mismatch with the observed bands in the experimental absorption spectra. This could be ascribed to the solvent effect and intermolecular bowl-to-bowl interactions which are not accounted for by the TD-DFT B3LYP level of theory. Despite all this, the calculated maximum wavelength of

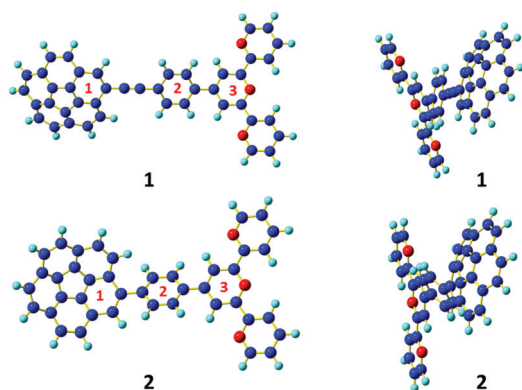


Fig. 10 B3LYP/6-31G\* calculated geometries for **1** (top) and **2** (bottom).

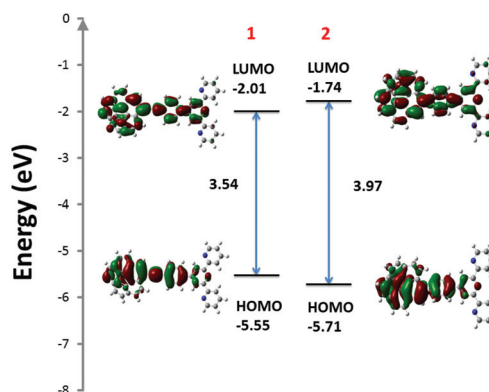


Fig. 11 A schematic representation of the molecular orbitals for **1** and **2**.

**Table 3** Calculated TD-DFT wavelengths (nm) and oscillator strengths (*f*) for **1** and **2**

Compound	Calculated wavelength/nm	<i>f</i>
<b>1</b>	403.74	1.0101
	383.81	0.0022
	366.46	0.2513
<b>2</b>	361.95	0.0366
	351.43	0.0083

ligand **1** is red-shifted with respect to the calculated maximum wavelength of ligand **2**, which is concordant with the results observed in the experimental absorption spectra.

## Conclusions

In summary, the first two terpyridine ligands based on corannulene (**1** and **2**) were synthesized *via* the Kröhnke condensation reaction as well as palladium-catalyzed coupling reactions. Both the title compounds are examined spectroscopically and displayed characteristic absorption and emission profiles. Ligand **1** exhibits a bathochromic shift in its absorption spectra and shows a higher fluorescence quantum yield than ligand **2**, suggesting that the acetylene bridge enhances the conjugation of the molecule and enables more efficient energy transfer.

The metal sensing properties of the ligands were investigated by visual examination, UV-vis and fluorescence measurements. **1** and **2** exhibit colorimetric sensing ability for Fe<sup>2+</sup> through an obvious color change which is from colorless to magenta, and this color change could be observed easily by the naked eye. Comparison of the binding constants of the two ligands suggests that the conjugated size of the substitute group plays a vital role in the binding ability of terpyridine to metal ions, which could be used for designing novel tunable chemosensors.

Moreover, both ligands also functioned as fluorimetric sensors for biologically related Zn<sup>2+</sup> by eliciting a significant bathochromic shift of around 60 nm in the emission maximum, which facilitates the discrimination of Zn<sup>2+</sup> from other metal ions. More specific quantitative studies reveal that the ligands coordinate Fe<sup>2+</sup> or Zn<sup>2+</sup> with a 1:1 complexation stoichiometry. These characteristics make **1** and **2** attractive for potential applications as multifunctional optical or colorimetric sensors for multiple analytes of Fe<sup>2+</sup> and Zn<sup>2+</sup>.

## Acknowledgements

This work was supported by the Ministry of Education Project combining the Industry and Teaching with Research of Guangdong Province (no. 2011B090400062).

## Notes and references

- L. M. Hyman and K. J. Franz, *Coord. Chem. Rev.*, 2012, **256**, 2333.
- B. Valeur and I. Leray, *Coord. Chem. Rev.*, 2000, **205**, 3.
- A. P. de Silva, H. Q. N. Gunaratne, T. Gunnlaugsson, A. J. M. Huxley, C. P. McCoy, J. T. Rademacher and T. E. Rice, *Chem. Rev.*, 1997, **97**, 1515.
- M. Zheng, H. Tan, Z. Xie, L. Zhang, X. Jing and Z. Sun, *ACS Appl. Mater. Interfaces*, 2013, **5**, 1078.
- M. Kumar, N. Kumar and V. Bhalla, *Dalton Trans.*, 2013, **42**, 981.
- J. Y. Koh, S. W. Suh, B. J. Gwag, Y. Y. He, C. Y. Hsu and D. W. Choi, *Science*, 1996, **272**, 1013.
- A. I. Bush, W. H. Pettingell, G. Multhaupt, M. d. Paradis, J. P. Vonsattel, J. F. Gusella, K. Beyreuther, C. L. Masters and R. E. Tanzi, *Science*, 1994, **265**, 1464.
- H. Hofmeier and U. S. Schubert, *Chem. Soc. Rev.*, 2004, **33**, 373.
- E. Baranoff, J.-P. Collin, L. Flamigni and J.-P. Sauvage, *Chem. Soc. Rev.*, 2004, **33**, 147.
- T. Vitvarová, J. Zedník, M. Bláha, J. Vohlídal and J. Svoboda, *Eur. J. Inorg. Chem.*, 2012, 3866.
- W. Goodall and J. A. G. Williams, *Chem. Commun.*, 2001, 2514.
- C. Hadad, S. Achelle, I. López-Solera, J. C. García-Martínez and J. Rodríguez-López, *Dyes Pigm.*, 2013, **97**, 230.
- S. Yin, J. Zhang, H. Feng, Z. Zhao, L. Xu, H. Qiu and B. Tang, *Dyes Pigm.*, 2012, **95**, 174.
- Y. Hong, S. Chen, C. W. T. Leung, J. W. Y. Lam, J. Liu, N.-W. Tseng, R. T. K. Kwok, Y. Yu, Z. Wang and B. Z. Tang, *ACS Appl. Mater. Interfaces*, 2011, **3**, 3411.
- F. A. Murphy and S. M. Draper, *J. Org. Chem.*, 2010, **75**, 1862.
- Y. T. Wu and J. S. Siegel, *Chem. Rev.*, 2006, **106**, 4843.
- V. M. Tsefrikas and L. T. Scott, *Chem. Rev.*, 2006, **106**, 4868.
- N. Niamnont, N. Kimpitak, K. Wongravee, P. Rashatasakhon, K. K. Baldrige, J. S. Siegel and M. Sukwattanasinitt, *Chem. Commun.*, 2013, **49**, 780.
- W. Li, X. Zhou, W. Q. Tian and X. Sun, *Phys. Chem. Chem. Phys.*, 2013, **15**, 1810.
- L. Zoppi, L. Martin-Samos and K. K. Baldrige, *J. Am. Chem. Soc.*, 2011, **133**, 14002.
- A. V. Zabula, A. S. Filatov, S. N. Spisak, A. Y. Rogachev and M. A. Petrukhina, *Science*, 2011, **333**, 1008.
- D. Miyajima, K. Tashiro, F. Araoka, H. Takezoe, J. Kim, K. Kato, M. Takata and T. Aida, *J. Am. Chem. Soc.*, 2009, **131**, 44.
- A. Sygula, F. R. Fronczek, R. Sygula, P. W. Rabideau and M. M. Olmstead, *J. Am. Chem. Soc.*, 2007, **129**, 3842.
- J. Mack, P. Vogel, D. Jones, N. Kaval and A. Sutton, *Org. Biomol. Chem.*, 2007, **5**, 2448.
- F. Kröhnke, *Synthesis*, 1976, 1.
- A. Wild, A. Winter, F. Schlutter and U. S. Schubert, *Chem. Soc. Rev.*, 2011, **40**, 1459.

- 27 H. Doucet and J.-C. Hierro, *Angew. Chem., Int. Ed.*, 2007, **46**, 834.
- 28 N. Kambe, T. Iwasaki and J. Terao, *Chem. Soc. Rev.*, 2011, **40**, 4937.
- 29 A. Sygula, G. Xu, Z. Marcinow and P. W. Rabideau, *Tetrahedron*, 2001, **57**, 3637.
- 30 A. Sygula and P. W. Rabideau, *J. Am. Chem. Soc.*, 2000, **122**, 6323.
- 31 J. Dey, A. Will, R. Agbaria, P. Rabideau, A. Abdourazak, R. Sygula and I. Warner, *J. Fluoresc.*, 1997, **7**, 231.
- 32 Z.-Q. Liang, C.-X. Wang, J.-X. Yang, H.-W. Gao, Y.-P. Tian, X.-T. Tao and M.-H. Jiang, *New J. Chem.*, 2007, **31**, 906.
- 33 Z.-B. Zheng, Z.-M. Duan, J.-X. Zhang and K.-Z. Wang, *Sens. Actuators, B*, 2012, **169**, 312.
- 34 A. Graczyk, F. A. Murphy, D. Nolan, V. Fernandez-Moreira, N. J. Lundin, C. M. Fitchett and S. M. Draper, *Dalton Trans.*, 2012, **41**, 7746.
- 35 Z.-X. Han, X.-B. Zhang, Z. Li, Y.-J. Gong, X.-Y. Wu, Z. Jin, C.-M. He, L.-X. Jian, J. Zhang, G.-L. Shen and R.-Q. Yu, *Anal. Chem.*, 2010, **82**, 3108.
- 36 Y. Ding, X. Li, T. Li, W. Zhu and Y. Xie, *J. Org. Chem.*, 2013, **78**, 5328.
- 37 Y. Xie, Y. Ding, X. Li, C. Wang, J. P. Hill, K. Ariga, W. Zhang and W. Zhu, *Chem. Commun.*, 2012, **48**, 11513.
- 38 M. J. Frisch, G. W. Trucks, H. B. Schlegel, G. E. Scuseria, M. A. Robb, J. R. Cheeseman, G. Scalmani, V. Barone, B. Mennucci, G. A. Petersson, H. Nakatsuji, M. Caricato, X. Li, H. P. Hratchian, A. F. Izmaylov, J. Bloino, G. Zheng, J. L. Sonnenberg, M. Hada, M. Ehara, K. Toyota, R. Fukuda, J. Hasegawa, M. Ishida, T. Nakajima, Y. Honda, O. Kitao, H. Nakai, T. Vreven, J. J. A. Montgomery, J. E. Peralta, F. Ogliaro, M. Bearpark, E. B. J. J. Heyd, K. N. Kudin, V. N. Staroverov, T. Keith, R. Kobayashi, J. Normand, K. Raghavachari, A. Rendell, J. C. Burant, S. S. Iyengar, J. Tomasi, M. Cossi, N. Rega, J. M. Millam, M. Klene, J. E. Knox, J. B. Cross, V. Bakken, C. Adamo, J. Jaramillo, R. Gomperts, R. E. Stratmann, O. Yazyev, A. J. Austin, R. Cammi, C. Pomelli, J. W. Ochterski, R. L. Martin, K. Morokuma, V. G. Zakrzewski, G. A. Voth, P. Salvador, J. J. Dannenberg, S. Dapprich, A. D. Daniels, O. Farkas, J. B. Foresman, J. V. Ortiz, J. Cioslowski and D. J. Fox, *GAUSSIAN 09 (Revision B.01)*, Gaussian, Inc., Wallingford, CT, 2010.